

polymer papers

Crystal structures, phase transitions and energy calculations of poly(*p*-phenylene) oligomers

Kenneth N. Baker, Albert V. Fratini, Timothy Resch and
Howard C. Knachel

Department of Chemistry, University of Dayton, Dayton, OH 45469-2357, USA

and W. W. Adams

Wright Laboratory, Materials Directorate, Wright-Patterson Air Force Base,
OH 45433-6533, USA

and E. P. Soggi and B. L. Farmer*

Department of Materials Science and Engineering, University of Virginia, Charlottesville,
VA 22903-2442, USA

(Received 9 July 1992)

The room temperature crystal structures, unit cell dimensions at 110 K and phase transitions of three poly(*p*-phenylene) oligomers are reported. The structures of *p*-quinquephenyl (PQP), C₃₀H₂₂, *p*-sexiphenyl (PSP), C₃₆H₂₆, and *p*-septiphenyl (PSeptiP), C₄₂H₃₀, each belonging to space group P2₁/c, are similar to those of shorter oligomers. The unit cell dimensions are $a=22.056$ Å, $b=5.581$ Å, $c=8.070$ Å and $\beta=97.91^\circ$ for PQP, $a=26.241$ Å, $b=5.568$ Å, $c=8.091$ Å and $\beta=98.17^\circ$ for PSP, and $a=30.577$ Å, $b=5.547$ Å, $c=8.034$ Å and $\beta=100.52^\circ$ for PSeptiP. The a axis increases with molecular length. The molecules are linear and planar in all three structures. The herringbone nature of the packing is similar for PQP and PSeptiP, while a considerably greater tilt occurs in PSP. At 110 K, the unit cell parameters b and c are approximately doubled while a remains nearly the same as in the room temperature cell. A time-dependent solid state transition is observed for PQP, PSP and PSeptiP when crystals are cooled to 110 K. At elevated temperatures, thermal measurements indicate the oligomers to be thermotropic liquid crystals. The crystal-smectic transition temperatures are reported for PQP, PSP, PSeptiP and *p*-octiphenyl (POP), C₄₈H₃₄. The results of a molecular mechanics study on the conformation and packing of PSP are also presented. The competition between intramolecular forces (such as *ortho* hydrogen repulsions) and intermolecular crystal packing forces was examined in particular. Molecular mechanics calculations predict non-planar conformations in isolated polyphenyls, implying that conjugation between phenyl rings is insufficient to overcome *ortho* hydrogen repulsions. In a crystalline environment, however, intermolecular forces tend to force a planar conformation. Calculations on arrays of PSP molecules show that changing the phenyl-phenyl torsion angles from the coplanar value increases the total energy of the structure. The most favourable intermolecular interactions between oligomers are achieved for conformations having the phenyl rings coplanar.

(Keywords: crystal structure; phase transitions; oligomer; poly(*p*-phenylene); molecular mechanics)

INTRODUCTION

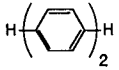
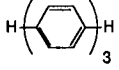
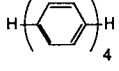
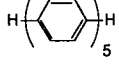
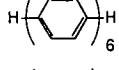
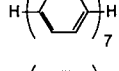
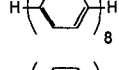
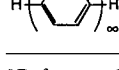
Poly(*p*-phenylene) (PPP) has been reviewed quite extensively¹⁻³. It is an insoluble and infusible dark brown material often referred to as 'brick dust'. Stated more positively, PPP has excellent heat and solvent stability. While its lower linear oligomers (shown in *Table 1*) and derivatives with phenyl pendant groups⁴ exhibit measurable melting points and limited solubilities, *p*-phenylenes are difficult to process. Nevertheless, the uses of PPP range from solid state lubricants⁵⁻⁸ to fibres⁹ and ribbons¹⁰. Objects made from PPP powder exhibit ablation-compaction properties which allow fabricated parts to undergo controlled uniform shrinkage up to

80%¹¹. Tensile bars fabricated from PPP powder by powder-forming techniques¹² and hydrostatic pressing¹³ exhibit tensile strengths as high as 35 MPa (5000 psi). In general, the mechanical properties of fabricated PPP fall between those of polyimide and graphite¹³. Calculations^{14,15} indicate that a high molecular weight PPP fibre would possess an excellent tensile modulus and compressive strength, the latter surpassing those of poly(*p*-phenylene benzobisoxazole) (PBO) and poly(*p*-phenylene benzobisthiazole) (PBZT).

PPP becomes a highly conducting n- or p-type material when it complexes, respectively, with either electron donors (Na, K or Li) or acceptors (AsF₅, SbF₅, BF₃ or PF₆)¹⁶. The highest conductivity occurs with AsF₅, where the conductivity increases from approximately

* To whom correspondence should be addressed

Table 1 PPP oligomer melting points and solubility

Oligomer	Melting point (°C)	Solubility (g l ⁻¹)
	70 ^a	440 in toluene ^a
	210 ^a	8.5 in toluene ^a
	320 ^a	0.22 in toluene ^a
	395 ^a 388 ^b 388 ^c	<0.1 in toluene ^a Good in 1,2,4-TCB ^b Unavailable ^c
	475 ^a 437 ^b 429 ^c	<0.01 in toluene ^a Poor in 1,2,4-TCB ^b Unavailable ^c
	545 ^a 468 ^b	Insoluble ^a Very limited in 1,2,4-TCB ^b
	491 ^b	Very limited in 1,2,4-TCB ^b
	Infusible ^d	Insoluble ^d

^a Reference 63^b Reference 64^c Reference 65^d Reference 51

1,2,4-TCB = 1,2,4-trichlorobenzene

10⁻¹² S m⁻¹ for the virgin polymer to greater than 10⁴ S m⁻¹ for the doped polymer — an increase of 16 orders of magnitude!

Different models have been proposed for the two types of conducting materials. An intercalation model has been suggested¹⁷ based on the diffraction pattern obtained from PPP heavily doped with AsF₅. Fibres of PPP increased in diameter by approximately 50% upon doping, suggesting diffusion of dopant molecules into the fibre. An alternate model¹⁸ proposed that the K⁺ ions aggregate in columns between two parallel polymer chains. In this model, the K⁺ ions stack over the midpoint of the HC-CH bonds parallel to the molecular axis rather than stack over the centres of the phenyl rings. This model is consistent with the suggestion that PPP conduction is strongly influenced by the ability of the molecule to form the quinoid resonance structure^{19,20}. This influence comes about because the quinoid resonance structure would have greater electron density over the HC-CH bonds parallel to the molecular axis, in contrast to the benzoid structure with toroids of π electrons above and below the planes of the phenyl rings.

The electronic properties of PPP suggest that it might also have good non-linear optical (NLO) properties. Calculations^{19,21} on the electronic band structures of *p*-quaterphenyl, *p*-quaterpyrrole and *p*-quaterthiophene indicate that undoped PPP oligomer is more polarizable than its heteroatom counterparts. Moreover, the polarizabilities of all three oligomers increase when they are doped with sodium. The largest increase is in *p*-quaterphenyl, which doubles its mean polarizability to 159 eV and almost triples its linear polarizability along

the molecular axis to 790 eV. The scaling relationship¹⁹ between the linear polarizability and the third-order polarizability suggests that an even larger increase may occur for the third-order polarizability.

PPP has a band-gap of 3.2 eV²⁰. The band-gap is decreased by increasing the oligomer length²² and increasing the quinoid character of the oligomer backbone²³. Calculations^{24,25}, optical measurements²⁶, and electron paramagnetic resonance (e.p.r.) studies²⁷ demonstrate that upon heavy doping with alkali metals or AsF₅, spinless bipolarons are formed in coexistence with polarons. Optical measurements²³ suggest a polaron-exciton defect to occur over about five phenyl rings. Thus, an understanding of the structures of PPP oligomers in this size range may be especially important in elucidating the mechanism of the NLO properties of these materials.

Since PPP is the simplest type of rigid-rod polymer, it represents the least complicated case of shape anisotropy. According to Irvine *et al.*²⁸ 'These homologues (of PPP) offer unique examples that (i) are rigid with respect to the rectilinear axis, (ii) are effectively cylindrically symmetric about this axis, and (iii) are devoid of possible vitiating effects of polar groups.' Theoretical calculations have addressed the relationship of shape anisotropy to intermolecular forces²⁹. Since PPP oligomers are thermotropic liquid crystals, experiments³⁰ have been devoted to providing better understanding, and possible utilization, of the liquid crystal transitions.

X-ray data reveal that PPP and several of its oligomers adopt conformations such that the phenyl rings within each molecule are, on average, coplanar but undergo librational motion³¹⁻³⁴. *Isolated* molecules of biphenyl or *p*-terphenyl achieve their lowest energy conformations when each adopts intramolecular torsion angles of approximately 45 and 50°, respectively^{35,36}. In the crystal, the observed planarity is thought to result from the averaging over all of the rotational degrees of freedom belonging to the phenyl units within the oligomer. A double well potential, resulting from competition between intramolecular and intermolecular forces, has been proposed^{33,35} to describe the energy in a crystalline environment. This competition is between two effects: intramolecular repulsion between *ortho* hydrogen atoms on adjacent phenyl rings, and intermolecular packing forces which tend to restore planarity in order to optimize packing between molecules³⁵. Judging from the energy barriers calculated for isolated polyphenyls, the intermolecular forces present within the crystal must be significant³⁶.

We report the room temperature crystal structures, the low temperature unit cell dimensions, and phase transitions of *p*-quinquephenyl (PQP), *p*-sexiphenyl (PSP) and *p*-septiphenyl (PSeptiP). Results are also presented from a molecular modelling study of the roles of intra- and intermolecular interaction in determining the structures and conformations of PPP oligomers.

EXPERIMENTAL

Polycrystalline samples of PQP, PSP and PSeptiP were purified by sublimation or recrystallization. Density measurements were made by flotation in a solvent mixture containing dichloromethane (density, $d = 1.326$ g cm⁻³) and methanol ($d = 0.791$ g cm⁻³).

Single crystals were mounted on an Enraf-Nonius

Table 2 Potential functions for non-bonded interactions^a

Interaction	A (kcal mol ⁻¹)	B (Å ⁻¹)	C (kcal mol ⁻¹ Å ⁶)
C-C	14 961.4	3.09	640.18
H-H	2 647.02	3.74	27.33
C-H	4 315.8	3.415	138.1

^a Parameters are for the equation: $E(r) = A \exp(-Br) - Cr^{-6}$

CAD4 diffractometer interfaced to a DEC Micro PDP-11 computer. Diffraction intensities were collected at approximately 295 K. Unit cell parameters for low temperature phases were obtained at 110 K. The crystal was cooled using the Enraf-Nonius FR558 liquid nitrogen cryostat.

Reflection data were processed on a VAX 11/730 computer using the Structure Determination Package

Table 3 Crystallographic data

	<i>p</i> -Quinquephenyl	<i>p</i> -Sexiphenyl	<i>p</i> -Septiphenyl
Formula	C ₃₀ H ₂₂	C ₃₆ H ₂₆	C ₄₂ H ₃₀
FW	382.51	458.61	534.71
Melting point (°C)	388	437	468
Crystal system	Monoclinic	Monoclinic	Monoclinic
Space group	P2 ₁ /c	P2 ₁ /c	P2 ₁ /c
Z	2	2	2
<i>a</i> (Å)	22.056(4)	26.241(5)	30.577(2)
<i>b</i> (Å)	5.581(1)	5.568(1)	5.547(3)
<i>c</i> (Å)	8.070(1)	8.091(3)	8.034(5)
α (deg)	90.0	90.0	90.0
β (deg)	97.91(1)	98.17(2)	100.52(5)
γ (deg)	90.0	90.0	90.0
Volume (Å ³)	982.9(5)	1170.2(8)	1339.9(8)
Density _{cal} (g cm ⁻³)	1.292	1.302	1.325
Density _{exp} (g cm ⁻³)	1.291	1.288	1.311
Crystal dimensions (mm)	0.29 × 0.28 × 0.05	0.35 × 0.50 × 0.05	0.10 × 0.10 × 0.50
Crystal shape	Flat plate	Rectangular plate	Needle
Cell determined	25 reflections 9° < 2θ < 36°	25 reflections 9° < 2θ < 25°	25 reflections 18° < 2θ < 58°
Radiation	Mo (graphite)	Mo (graphite)	Mo (graphite)
Scan type	ω/2θ	ω/2θ	ω/2θ
Scan rate (deg min ⁻¹)	1.27–5.49	1.27–5.49	1.27–5.49
Scan angle (deg)	0.80 + 0.34 tan θ	0.80 + 0.34 tan θ	0.80 + 0.34 tan θ
Power (kV/ma)	45/20	45/20	45/20
Collimator (mm)	1.3	1.3	1.3
Detector aperture (mm)	4.00	4.00	4.00
Check reflections	3 every 200 refl. 12° < 2θ < 24°	3 every 200 refl. 12° < 2θ < 24°	3 every 200 refl. 22° < 2θ < 26°
Orientation reflections	3 every 2 h 16° < 2θ < 36°	3 every 2 h 18° < 2θ < 24°	3 every 2 h 22° < 2θ < 26°
Temperature (°C)	22	22	22
2θ Range (deg)	2–50	2–50	2–50
Data collected, <i>h</i> , <i>k</i> , <i>l</i>	±31, 0–7, ±11	±31, 0–6, ±9	0–36, ±6, ±9
Total number of reflections	5776	4593	13 098
Unique number of reflections > 3σ	663	623	536
Number of parameters varied	136	163	230
Average decay correction	1.006	1.004	1.004
Absorption coefficient (cm ⁻¹)	0.7	0.7	0.7
Absorption correction	None	None	None
R ^a	0.050	0.062	0.103
RW ^b	0.060	0.091	0.093
Maximum shift/error in final cycle	0.03	0.01	0.03

$$^a R = \frac{\sum |F_o| - |F_c|}{\sum |F_o|}$$

$$^b RW = \sqrt{\frac{\sum W(|F_o| - |F_c|)^2}{\sum W(F_o)^2}}$$

(SDP)³⁷. Structure solutions were obtained using MULTAN 11/82³⁸ and/or SHELXS-86³⁹. Refinement was by full matrix least-squares, with hydrogen atoms in idealized positions. Subsequent isotropic refinement of hydrogen atoms did not yield appreciably better results.

A temperature programmable Enraf-Nonius FR553 Guinier-Simon camera equipped with an Enraf-Nonius FR558 liquid nitrogen cryostat was used to obtain variable low temperature structural data on PQP, PSP and PSeptiP. The moving film/ramping temperature option on the camera's controller allowed the determination of structural transition temperatures. Differential scanning calorimetry (d.s.c.) measurements were performed on a Dupont 910 apparatus interfaced with an Omnitherm 35053 three module controller.

COMPUTATIONAL METHOD

Molecular mechanics (MM) calculations were made using the SYBYL molecular modelling software package⁴⁰ running on a DEC MicroVAX II and an IBM RS/6000 computer. PSP models were constructed from the fractional coordinates determined by X-ray analysis. Their energies were minimized using the SYBYL force field and parameters⁴¹ modified to reproduce the torsional barrier calculated using semiempirical molecular orbital methods⁴².

Calculations of the intermolecular energies of pairs and arrays of PSP molecules were made using a crystal energy minimization program (CREAM) which calculates non-bonded van der Waals interactions for molecules having fixed geometry⁴³. Parameters used for the non-bonded potentials⁴⁴ are presented in Table 2. The non-bonded cut-off distance was set at 10 Å. Energy contour maps were made using SURFER⁴⁵.

The molecular modelling investigation analyses the

packing energy for PSP oligomers having various regular conformations. In order to determine their optimal orientations with respect to one another, calculations were first made on identical pairs of PSP oligomers constrained at the desired phenyl-phenyl torsion angles. Both angular orientations (setting angles) and translations along the molecular axis were examined for molecules constrained to having parallel molecular axes. Further calculations evaluated the energy of an array of seven PSP oligomers as the phenyl-phenyl torsion angles of the oligomers were varied. Unit cell axes, angles and setting angles were varied simultaneously and optimized for selected conformations.

X-RAY RESULTS AND DISCUSSION

Table 3 summarizes the crystallographic results for the room temperature structures. Experimental problems prevented the collection of complete data sets at 110 K. Space group and unit cell information for the room and low temperature polyphenyls are summarized in Table 4.

The PQP, PSP and PSeptiP molecules pack in herringbone structures which leave the molecular axes parallel but the molecular planes non-parallel. This type of structure is also observed in the lower oligomers³¹. The carbon atoms of the PQP asymmetric unit are labelled in Figure 1. Each hydrogen atom was numbered the same as the carbon atom to which it was attached. Tables 5 and 6 list the atomic positions, bond lengths and bond angles for PQP. Figure 2 shows a stereoview of the crystal packing in the unit cell. PSP is shown in Figure 3 with atomic positions presented in Table 7 and bond lengths and bond angles in Table 8. The stereodrawing of the crystal packing within the unit cell is shown in Figure 4. The PSeptiP molecule is shown in Figure 5. Atomic positions, bond lengths and bond angles

Table 4 Unit cell parameters

Compound	Temperature (K)	Space group	a (Å)	b (Å)	c (Å)	α (deg)	β (deg)	γ (deg)
Biphenyl	298 ^a	P2 ₁ /c ^f	9.51(2)	5.63(1)	8.12(2)	90	95.1(3)	90
	40 ^b	P2 ₁ /c ^f	9.51(2)	11.26(2)	16.24(4)	90	95.1(3)	90
<i>p</i> -Terphenyl	298 ^c	P2 ₁ /c ^f	13.613(6)	5.613(2)	8.106(4)	90	92.2(2)	90
	191 ^c	P2 ₁ /c ^{fg}	13.53(3)	11.09(3)	16.01(3)	90	92.0(2)	90
<i>p</i> -Quaterphenyl	295 ^d	P2 ₁ /c ^f	17.91(1)	5.610(4)	8.110(6)	90	95.80(6)	90
	243 ^e	P2 ₁ /c ^{fg}	17.70(3)	11.16(2)	15.97(3)	90	95.61(8)	90
<i>p</i> -Quinquephenyl	298	P2 ₁ /c	22.056(4)	5.581(1)	8.070(1)	90	97.91(1)	90
	110	Monoclinic, C centred	22.014(3)	11.029(4)	15.968(6)	90	98.18(2)	90
<i>p</i> -Sexiphenyl	295	P2 ₁ /c	26.241(5)	5.568(1)	8.091(3)	90	98.17(2)	90
	110	Monoclinic, C centred	26.282(8)	10.999(4)	15.995(9)	90	99.79(4)	90
<i>p</i> -Septiphenyl	295	P2 ₁ /c ^f	30.577(2)	5.547(3)	8.034(5)	90	100.52(5)	90
	110	Orthorhombic, C centred	30.064(6)	11.005(2)	15.972(2)	90	90	90

^a Reference 57

^b Reference 55

^c Reference 56

^d Reference 66

^e Reference 32

^f For comparison purposes, the P2₁/a space groups were transformed to P2₁/c

^g Space group of structure refinement is P1 and is converted to a pseudo-monoclinic cell with molecules centred on the (001) face for comparison purposes

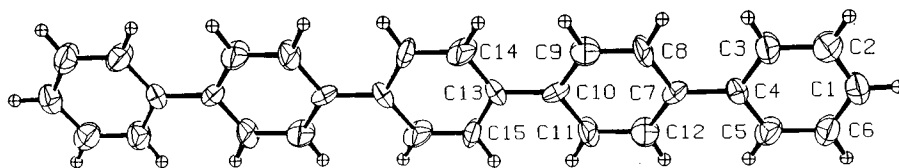


Figure 1 *p*-Quinquephenyl with carbon atom ellipsoids drawn at the 50% probability level

Table 5 Positional parameters, equivalent isotropic thermal factors and their estimated standard deviations for *p*-quinquephenyl

Atom	<i>x</i>	<i>y</i>	<i>z</i>	<i>B</i> (Å ²) ^a
C1	0.4390(2)	−0.0065(9)	0.2967(5)	4.1(1)
C2	0.3989(2)	−0.1807(9)	0.2300(5)	4.6(1)
C3	0.3384(2)	−0.1788(9)	0.2567(5)	4.1(1)
C4	0.3163(2)	0.0007(8)	0.3521(4)	2.63(8)
C5	0.3572(2)	0.1761(8)	0.4183(5)	4.2(1)
C6	0.4180(2)	0.1739(9)	0.3906(5)	4.4(1)
C7	0.2515(2)	0.0042(7)	0.3830(4)	2.71(8)
C8	0.2115(2)	−0.1726(9)	0.3206(6)	5.1(1)
C9	0.1511(2)	−0.1737(8)	0.3475(5)	4.8(1)
C10	0.1263(2)	−0.0020(7)	0.4393(4)	2.62(8)
C11	0.1663(2)	0.1751(9)	0.5007(6)	4.8(1)
C12	0.2267(2)	0.1775(9)	0.4743(5)	5.0(1)
C13	0.0614(2)	−0.0037(7)	0.4698(4)	2.59(7)
C14	0.0204(2)	−0.1789(8)	0.4079(5)	4.6(1)
C15	0.0397(2)	0.1773(9)	0.5622(5)	4.3(1)
H1	0.481	−0.012	0.281	5.4*
H2	0.413	−0.302	0.162	6.0*
H3	0.312	−0.302	0.209	5.3*
H5	0.343	0.299	0.485	5.5*
H6	0.445	0.297	0.436	5.4*
H8	0.226	−0.301	0.260	6.6*
H9	0.125	−0.298	0.298	6.2*
H11	0.152	0.304	0.562	6.1*
H12	0.253	0.302	0.523	6.9*
H14	0.034	−0.297	0.337	5.8*
H15	0.066	0.305	0.601	5.1*

^a Asterisked atoms were refined isotropically. Anisotropically refined atoms are given in the form of the isotropic equivalent displacement parameter defined as:

$$(4/3)[a^2B_{1,1} + b^2B_{2,2} + c^2B_{3,3} + ab(\cos \gamma)B_{1,2} + ac(\cos \beta)B_{1,3} + bc(\cos \alpha)B_{2,3}]$$

are presented in Tables 9 and 10. Figure 6 shows a stereoview of the unit cell packing.

The unit cell parameters of the *n*=5, 6 and 7 polyphenylene oligomers (where *n* is the number of phenyl units in the molecule) agree well with the *n*=2, 3 and 4 oligomers (namely, biphenyl, *p*-terphenyl and *p*-quaterphenyl), allowing for space group transformations (see Table 4). The length of the *a* axis increases by approximately 4.14 Å with the addition of each phenyl group. This is less than the length of the phenyl structural unit which is approximately 4.3 Å. Structural features that might account for this foreshortening are phenyl ring deformation (chain compression or expansion), molecular axis bending, or chain tilting with respect to the unit cell axis. These possibilities are discussed in greater detail later in this section.

The stereoviews of the oligomers in Figures 2, 4 and 6 reveal that the molecular axis is indeed tilted away from the long crystallographic axis. Biphenyl⁴⁶, *p*-terphenyl⁴⁷ and *p*-quaterphenyl⁴⁸ exhibit similar tilting. Figure 7 presents two different views of a PSeptiP unit cell showing how the molecules align with respect to the *ac* or (0 1 0) plane. The setting angle Θ is defined as the angle the phenyl planes of the 'averaged' oligomer make with the (0 1 0) face. The figure also shows

intersections of the molecular axes with the *ab* (0 0 1) and *bc* (1 0 0) planes, defining intersection angles ω and ϕ , respectively. Angular data are tabulated in Table 11. Note that $\omega + \phi$ is approximately equal to the β unit cell angle.

PPP has been found⁴⁹ to have $\Theta = 57^\circ$. This was determined by incorporating the setting angle into the data refinement and defining the molecular axes to be perpendicular to the (1 0 0) plane and parallel to the (0 1 0) and (0 0 1) planes. The average setting angle of $56.3 \pm 0.3^\circ$ observed here for the oligomers agrees very well with this value derived for the polymer. The intersection angle ϕ is constant at approximately $72 \pm 0.3^\circ$ and it does not approach the value of 90° found for PPP. The intersection angle ω fluctuates as the oligomer length increases. With the exception of PSP, ω decreases with oligomer length, approaching the value of zero found for PPP. It is not clear why PSP does not fit the trend of the other oligomers. PSP might have other polymorphs, and changing the conditions of crystallization could influence the crystal structure. It has been suggested⁵⁰ that PSP might serve as a good model for PPP, based on its very similar X-ray photoelectron spectrum. Based on its structure, in particular the intersection angle, this does not seem to be the case.

The PQP, PSP and PSeptiP molecules are centrosymmetric. The angles between the atoms constituting the molecular axis are shown in Table 12. The largest deviation from linearity occurs in PSP. Designating the terminal phenyl ring as 1, there is a 3.6° kink between phenyl rings 3 and 4 (at the centre of symmetry) and a 3.3° kink between phenyl rings 2 and 3.

The C–C bond lengths in the phenyl rings of PQP, PSP and PSeptiP agree quite well with expected values. The endocyclic bond angles of the chain axis carbon atoms are less than the ideal 120° . This is consistent with the structures^{46–48} of the lower oligomers. This results in narrowing and lengthening the rings, making the overall oligomer slightly longer than expected. PSP has the widest range (114.0 – 120.3°) of these endocyclic angles. The other bond angles agree well with expected values. From these observations, it is clear that chain tilting in the unit cell accounts for most of the discrepancy between the expected and observed incremental change in the *a* unit cell dimension for the sequence of oligomers. Ring deformation is also present, but the distortions are such as to lengthen the oligomers rather than to shorten them.

Fitting a least-squares plane to the carbon atoms of the asymmetric unit of each oligomer reveals that all of the phenyl rings of each molecule lie in the same plane in the room temperature structures of the oligomers. The largest deviation from the plane was 0.05 Å for C9 in PSeptiP. The planar structure can be interpreted as the average of all the rotational degrees of freedom belonging to the phenyl units. Librational tensors reported for the lower oligomers⁴⁷ reveal that the rings do have a high degree of torsional

Table 6 Bond distances (Å) and bond angles (deg) for *p*-quinquephenyl

Atom 1	Atom 2	Distance	Atom 1	Atom 2	Distance	Atom 1	Atom 2	Distance
C3	C4	1.392(6)	C10	C13	1.482(5)	C8	C9	1.376(6)
C3	C2	1.378(6)	C11	C12	1.373(6)	C1	C2	1.374(6)
C3	H3	0.950(4)	C11	H11	0.950(5)	C8	H8	0.951(5)
C4	C5	1.386(6)	C12	H12	0.951(4)	C1	C6	1.379(7)
C4	C7	1.481(5)	C13	C14	1.378(6)	C9	C10	1.372(6)
C5	C6	1.388(6)	C13	C15	1.380(6)	C1	H1	0.951(4)
C5	H5	0.951(5)	C14	C15'	1.378(6)	C9	H9	0.951(4)
C7	C8	1.372(6)	C14	H14	0.950(5)	C2	H2	0.950(5)
C7	C12	1.376(6)	C15	H15	0.950(4)	C6	H6	0.950(4)
C10	C11	1.373(6)	C15	C14'	1.378(6)			

Atom 1	Atom 2	Atom 3	Angle	Atom 1	Atom 2	Atom 3	Angle
C4	C3	C2	120.7(4)	C12	C11	H11	117.8(4)
C4	C3	H3	120.3(4)	C7	C12	C11	122.8(5)
C2	C3	H3	119.1(4)	C7	C12	H12	118.4(4)
C3	C4	C5	117.7(3)	C11	C12	H12	118.8(5)
C3	C4	C7	121.3(3)	C10	C13	C14	122.8(4)
C5	C4	C7	121.0(4)	C10	C13	C15	119.9(3)
C4	C5	C6	121.4(4)	C14	C13	C15	117.3(4)
C4	C5	H5	119.1(4)	C13	C14	C15'	122.0(4)
C6	C5	H5	119.5(4)	C13	C14	H14	117.7(4)
C4	C7	C8	120.9(4)	C15'	C14	H14	120.2(4)
C4	C7	C12	124.3(4)	C13	C15	C14'	120.8(4)
C8	C7	C12	114.9(4)	C13	C15	H15	119.0(4)
C7	C8	C9	122.1(4)	C14'	C15	H15	120.1(4)
C7	C8	H8	119.4(4)	C2	C1	C6	119.1(4)
C9	C8	H8	118.5(4)	C2	C1	H1	120.7(4)
C8	C9	C10	123.2(5)	C6	C1	H1	120.3(4)
C8	C9	H9	118.3(5)	C3	C2	C1	121.1(4)
C10	C9	H9	118.4(4)	C3	C2	H2	119.5(4)
C9	C10	C11	114.6(4)	C1	C2	H2	119.3(5)
C9	C10	C13	123.4(4)	C5	C6	C1	120.0(4)
C11	C10	C13	122.1(4)	C5	C6	H6	119.9(5)
C10	C11	C12	122.6(4)	C1	C6	H6	120.2(4)
C10	C11	H11	119.6(4)				

Numbers in parentheses are estimated standard deviations in the least significant digits

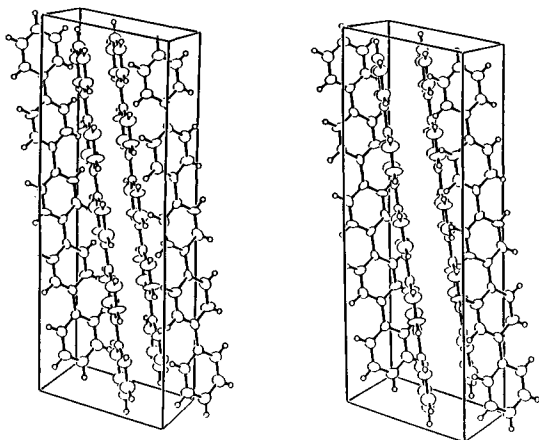


Figure 2 Stereoview of PQP showing the molecular packing in the unit cell. The *a* axis is vertical and the *b* axis is horizontal

motion, which is consistent with large $U(3,3)$ values for PQP, PSP and PSeptiP. The inter-ring torsion angles confirm the averaged coplanarity. Calculations of PPP conformations ignoring crystal packing forces¹⁴

indicate a lowest-energy conformation with the rings perpendicular to each other. Calculations on isolated biphenyl⁴² and terphenyl indicate inter-ring torsion angles of approximately 45–50°. This suggests that constraints within the unit cell might be strong enough to overcome the *ortho* hydrogen repulsions.

Although PPP is reported to be infusible⁵¹, its melting point can be determined by extrapolation of the melting points of these PPP oligomers. As shown in *Figure 8*, the melting point is expected to be about 1020 K. Using similar methods based on melting point depression associated with end group concentration in polymers⁵², melting points of 620 K and 1260 K have been reported for poly(tetrafluoroethylene)⁵³ and poly(*p*-phenylene terephthalamide)⁵⁴, respectively. It should be noted that all of these polymers are expected to degrade before reaching these theoretical melting points. Using calculated unit cell densities from crystalline oligomers, an extrapolated (see *Figure 9*) crystal density of 1.36 g cm⁻³ is expected for PPP. This theoretical density is lower than that measured for PBO and PBZT

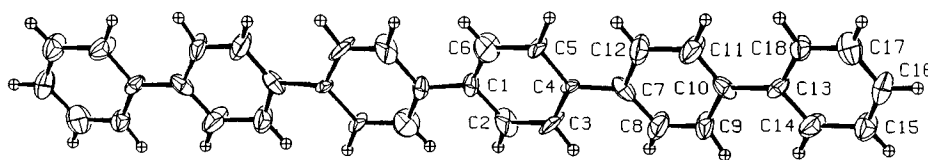


Figure 3 *p*-Sexiphenyl with carbon atom ellipsoids drawn at the 50% probability level

Table 7 Positional parameters, equivalent isotropic thermal factors and their estimated standard deviations for *p*-sexiphenyl

Atom	<i>x</i>	<i>y</i>	<i>z</i>	<i>B</i> (Å ²) ^a
C1	0.0276(2)	0.007(1)	0.0409(6)	2.5(1)
C2	0.0620(2)	-0.174(1)	0.0066(8)	4.5(2)
C3	0.1117(3)	-0.174(1)	0.0849(8)	4.5(2)
C4	0.1321(2)	0.001(1)	0.1953(6)	1.6(1)
C5	0.0982(2)	0.179(1)	0.2214(8)	3.9(2)
C6	0.0456(3)	0.179(2)	0.1529(9)	5.7(2)
C7	0.1875(3)	-0.008(1)	0.2729(7)	3.6(2)
C8	0.2220(3)	-0.181(2)	0.2399(9)	5.4(2)
C9	0.2696(2)	-0.178(1)	0.3188(8)	4.4(2)
C10	0.2910(2)	0.002(1)	0.4253(7)	3.1(1)
C11	0.2569(3)	0.175(1)	0.4563(9)	5.3(2)
C12	0.2051(2)	0.173(1)	0.3828(9)	4.6(2)
C13	0.3443(2)	0.001(1)	0.5074(7)	2.7(1)
C14	0.3781(2)	-0.174(1)	0.4752(8)	4.1(2)
C15	0.4320(2)	-0.177(2)	0.5448(9)	4.7(2)
C16	0.4488(3)	0.003(2)	0.6560(9)	5.3(2)
C17	0.4149(3)	0.179(2)	0.6951(9)	4.9(2)
C18	0.3661(2)	0.183(1)	0.6192(8)	3.4(1)
H2	0.052	-0.296	-0.074	5.2*
H3	0.133	-0.304	0.064	5.6*
H5	0.111	0.314	0.286	4.5*
H6	0.023	0.293	0.189	7.1*
H8	0.212	-0.293	0.153	6.8*
H9	0.290	-0.316	0.310	5.7*
H11	0.270	0.306	0.525	6.5*
H12	0.182	0.293	0.411	5.8*
H14	0.365	-0.306	0.408	5.8*
H15	0.455	0.291	0.510	5.1*
H16	0.484	0.005	0.707	6.4*
H17	0.426	0.295	0.779	6.6*
H18	0.345	0.316	0.639	4.2*

^a Asterisked atoms were refined isotropically. Anisotropically refined atoms are given in the form of the isotropic equivalent displacement parameter defined as:

$$(4/3)[a^2B_{1,1} + b^2B_{2,2} + c^2B_{3,3} + ab(\cos \gamma)B_{1,2} + ac(\cos \beta)B_{1,3} + bc(\cos \alpha)B_{2,3}]$$

(1.65 and 1.69 g cm⁻³, respectively). Since modulus is directly proportional to density, this result supports calculations^{14,15} which indicate that PPP fibres would have a lower modulus than PBO and PBZT.

Structural transitions

Studies of the lower polyphenyls^{32,55,56} have revealed that a structural transition occurs such that the 'averaged' planar conformation observed at room temperature changes to non-planar at lower temperatures. The low temperature unit cell is a superstructure of the room temperature cell, with the parameters *b* and *c* approximately doubled to account for the more three-dimensional nature and greater excluded volume of non-planar conformations. The temperatures of these crystalline transitions (indicated in Table 4) are plotted in Figure 10 along with the melting points of the PPP oligomers up to *p*-octiphenyl. The trend of the data suggests that the transition temperatures for PQP, PSP and PSeptiP should be near room temperature. However,

their room temperature structures are planar. Further, d.s.c. measurements indicate that no transitions occur until the vicinity of the melting point is reached. Upon cooling to 110 K, however, both PQP and PSP single crystals index to unit cells slightly larger than their room temperature unit cells. After approximately 1 day, a structural transition occurred (in each material) to a monoclinic unit cell where *b* and *c* were approximately doubled from the original cell dimensions. PSeptiP transformed (in about 2 h) to an orthorhombic unit cell with *b* and *c* approximately doubled from the original unit cell. Data sets initially obtained at low temperature were inadequate to allow the determination of the space groups or structures at low temperature, and further effort is underway.

PQP, PSP and PSeptiP apparently undergo a time-dependent phase transition. D.s.c. measurements on polycrystalline samples cooled at a rate of 10°C min⁻¹ showed no transition down to 133 K. Similarly, no transitions were observed in low temperature diffraction patterns taken after cooling the samples to 143 K and holding them there for as long as 5 days. The transition temperature must therefore be between 143 K and 110 K as indicated by the error bars in Figure 10. The transition itself is time dependent. This transition, which has a time dependency and which is much lower in temperature than those for the other polyphenyls, could be explained by a non-first-order phase transition such as that observed for biphenyl^{55,57} for which a soft mode exists below its transition temperature.

D.s.c. data on PQP, PSP, PSeptiP and *p*-octiphenyl (POP), shown in Figure 11a-d, respectively, indicate that the samples also undergo high temperature transitions near the melting point. These have been attributed to liquid crystal transitions. PQP shows a small peak at 418°C, probably indicating the nematic-isotropic transition after the melting point at 388°C. This is in agreement with previous reports^{30,58}. PSP likewise shows good agreement with previous results^{30,58}, with peaks at 410, 440 and 474°C, probably indicating high temperature crystal-crystal, crystal-smectic and smectic-nematic phase transitions, respectively. The crystal-crystal transition is observed at a higher temperature than reported previously⁵⁹. Decomposition of the sample precluded observation of the nematic-isotropic phase transition^{30,58}. The d.s.c. of PSeptiP shows three peaks at 420, 473 and 486°C, probably indicating the same sequence of transitions as in PSP.

The transition temperatures are plotted in Figure 12. Results from the literature^{30,59} are also plotted. If PSeptiP and POP follow the trend of the lower polyphenyls, their nematic-isotropic transitions could be as high as 700 and 800°C, respectively — much higher than the respective decomposition temperatures⁶⁰ of the oligomers. Study of the mesophase region would require special containment such as high-pressure, inert-atmosphere cells. In the temperature range between

Table 8 Bond distances (Å) and bond angles (deg) for *p*-sexiphenyl

Atom 1	Atom 2	Distance	Atom 1	Atom 2	Distance	Atom 1	Atom 2	Distance
C1	C1'	1.506(6)	C9	H9	0.951(7)	C5	H5	0.950(6)
C1	C2	1.41(1)	C10	C11	1.36(2)	C16	C17	1.39(1)
C1	C6	1.36(2)	C10	C13	1.461(8)	C6	H6	0.951(9)
C2	C3	1.366(9)	C11	C12	1.40(1)	C16	H16	0.950(8)
C2	H2	0.951(7)	C11	H11	0.950(7)	C7	C8	1.38(2)
C12	H12	0.950(7)	C17	C18	1.339(8)	C9	C10	1.386(9)
C3	C4	1.378(8)	C13	C14	1.37(1)	C7	C12	1.38(1)
C3	H3	0.950(7)	C13	C18	1.426(9)	C17	H17	0.951(8)
C4	C5	1.366(8)	C14	C15	1.446(9)	C8	C9	1.321(9)
C4	C7	1.501(8)	C14	H14	0.950(7)	C18	H18	0.950(7)
C15	C16	1.38(2)	C8	H8	0.950(8)	C15	H15	0.951(8)
C5	C6	1.413(9)						

Atom 1	Atom 2	Atom 3	Angle	Atom 1	Atom 2	Atom 3	Angle
C1'	C1	C2	118.7(6)	C8	C9	H9	117.2(7)
C1'	C1	C6	123.5(6)	C10	C9	H9	117.0(6)
C2	C1	C6	117.8(5)	C9	C10	C11	114.0(6)
C1	C2	C3	120.2(6)	C9	C10	C13	123.7(7)
C1	C2	H2	121.0(6)	C11	C10	C13	122.1(6)
C3	C2	H2	118.7(7)	C10	C11	C12	122.5(7)
C2	C3	C4	124.0(7)	C10	C11	H11	117.3(6)
C2	C3	H3	118.1(7)	C12	C11	H11	120.2(7)
C4	C3	H3	117.9(6)	C7	C12	C11	119.8(7)
C3	C4	C5	114.3(5)	C7	C12	H12	120.2(6)
C3	C4	C7	120.8(5)	C11	C12	H12	120.0(8)
C5	C4	C7	124.9(5)	C10	C13	C14	121.5(6)
C4	C5	C6	124.1(6)	C10	C13	C18	123.8(6)
C4	C5	H5	117.6(5)	C14	C13	C18	114.7(5)
C6	C5	H5	118.3(6)	C13	C14	C15	123.9(6)
C1	C6	C5	119.3(7)	C13	C14	H14	117.7(6)
C1	C6	H6	120.3(6)	C15	C14	H14	118.4(7)
C5	C6	H6	120.3(8)	C14	C15	C16	117.0(7)
C4	C7	C8	124.5(6)	C14	C15	H15	121.7(7)
C4	C7	C12	117.6(7)	C16	C15	H15	121.4(6)
C8	C7	C12	117.9(6)	C15	C16	C17	120.3(7)
C7	C8	C9	119.9(7)	C15	C16	H16	119.4(8)
C7	C8	H8	119.0(6)	C17	C16	H16	120.3(8)
C9	C8	H8	120.9(8)	C16	C17	C18	120.7(8)
C8	C9	C10	125.7(7)	C16	C17	H17	119.9(6)
C18	C17	H17	119.4(7)	C13	C18	C17	123.3(7)
C13	C18	H18	117.9(5)	C17	C18	H18	118.8(7)

Numbers in parentheses are estimated standard deviations in the least significant digits

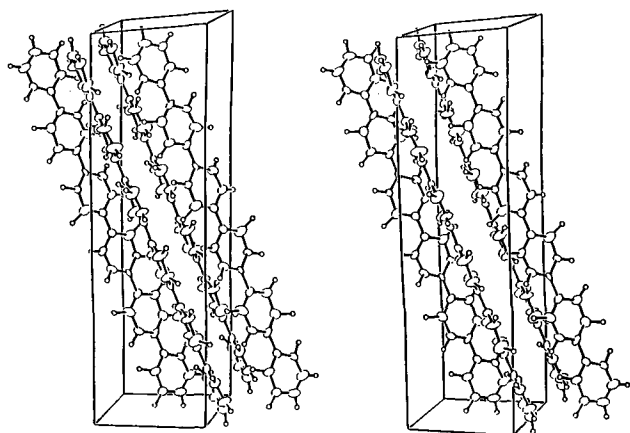


Figure 4 Stereoview of PSP showing the molecular packing in the unit cell. The *a* axis is vertical and the *b* axis is horizontal

the crystal-crystal transition and the transition to the isotropic melt, nuclear magnetic resonance (n.m.r.) studies^{61,62} indicate that the phenyl rings undergo 180° flips about the molecular axis in the amorphous phase. The rate of flipping, already rapid at room temperature, increases dramatically as the temperature increases. At low temperature, the magnitude of ring oscillations⁵⁸ decreases to about 20–30° and the low-temperature cell and structure dominate.

MODELLING RESULTS AND DISCUSSION

Isolated polyphenyls are non-planar^{35,36,42}. *Figure 13* shows a plot of intramolecular energy *versus* torsion angle for an isolated PSP oligomer. The molecular geometry used for the oligomer was that obtained in the X-ray

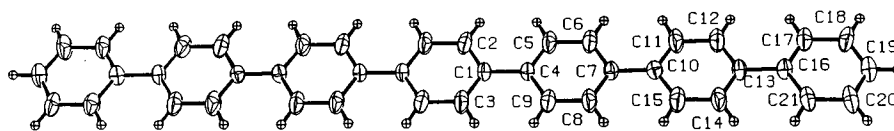


Figure 5 *p*-Septiphenyl with carbon atom ellipsoids drawn at the 50% probability level

Table 9 Positional parameters, equivalent isotropic thermal factors and their estimated standard deviations for *p*-septiphenyl

Atom	x	y	z	<i>B</i> (Å ²) ^a
C1	0.4550(1)	0.5003(7)	0.5218(4)	2.41(6)
C2	0.4719(1)	0.3218(9)	0.4321(6)	4.48(9)
C3	0.4842(1)	0.6798(9)	0.5876(5)	4.5(1)
C4	0.4078(1)	0.5009(7)	0.5437(4)	2.39(7)
C5	0.3786(1)	0.3223(8)	0.4757(5)	4.33(9)
C6	0.3347(1)	0.3206(9)	0.4966(5)	4.38(9)
C7	0.3178(1)	0.5007(7)	0.5860(4)	2.46(6)
C8	0.3470(1)	0.6783(9)	0.6525(6)	4.39(9)
C9	0.3910(1)	0.6784(8)	0.6331(5)	4.33(9)
C10	0.2709(1)	0.4993(8)	0.6086(4)	2.43(7)
C11	0.2415(1)	0.3226(9)	0.5415(6)	5.2(1)
C12	0.1977(1)	0.3224(9)	0.5607(6)	4.9(1)
C13	0.1808(1)	0.5012(8)	0.6496(4)	2.63(7)
C14	0.2098(1)	0.6772(9)	0.7158(6)	5.0(1)
C15	0.2539(1)	0.6767(9)	0.6975(6)	5.0(1)
C16	0.1333(1)	0.4997(9)	0.6722(4)	2.68(7)
C17	0.1041(1)	0.3212(9)	0.5993(5)	3.81(9)
C18	0.0595(1)	0.3234(9)	0.6197(5)	4.3(1)
C19	0.0445(1)	0.505(1)	0.7094(5)	3.93(9)
C20	0.0728(1)	0.682(1)	0.7841(6)	4.7(1)
C21	0.1173(1)	0.6782(9)	0.7621(5)	3.96(9)
H2	0.453	0.195	0.385	4.4*
H3	0.474	0.807	0.649	4.5*
H5	0.389	0.197	0.413	4.1*
H6	0.316	0.193	0.450	4.4*
H8	0.336	0.805	0.713	4.2*
H9	0.410	0.806	0.680	4.3*
H11	0.252	0.195	0.480	4.9*
H12	0.179	0.195	0.514	4.8*
H14	0.199	0.804	0.777	4.7*
H15	0.273	0.804	0.744	4.8*
H17	0.114	0.197	0.535	3.9*
H18	0.040	0.197	0.574	4.4*
H19	0.014	0.509	0.719	3.9*
H20	0.062	0.803	0.850	4.7*
H21	0.137	0.804	0.809	3.8*

^a Asterisked atoms were refined isotropically. Anisotropically refined atoms are given in the form of the isotropic equivalent displacement parameter defined as:

$$(4/3)[a^2B_{1,1} + b^2B_{2,2} + c^2B_{3,3} + ab(\cos \gamma)B_{1,2} + ac(\cos \beta)B_{1,3} + bc(\cos \alpha)B_{2,3}]$$

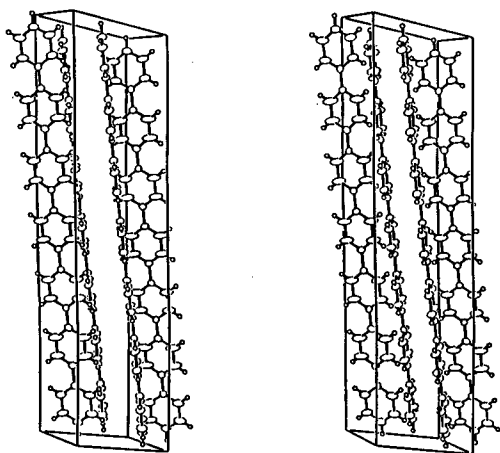


Figure 6 Stereoview of PSeptiP showing the molecular packing in the unit cell. The *a* axis is vertical and the *b* axis is horizontal

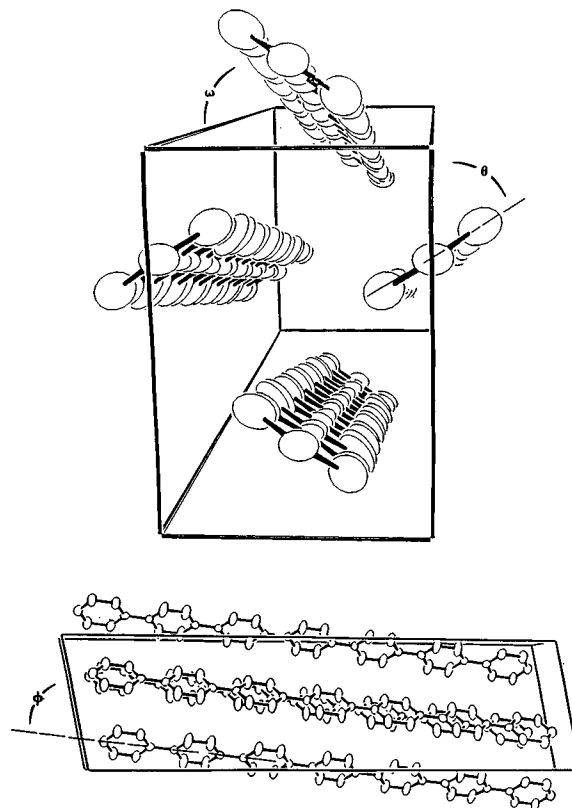


Figure 7 Perspective view of the oligomer structure, showing the setting angle and intersection angles

structure determination of PSP. Torsion angles were adjusted as needed, and in a fashion such that alternate rings down the chain remained coplanar. Bond lengths and angles retained their crystallographically determined values. The isolated molecule achieves its lowest energy when it is non-planar, having torsion angles in the range of 30–40°. This is consistent with results of AM1 calculations⁴² on biphenyl which show the minimum energy torsion angle to be 45–50° in a geometrically optimized molecule. Since the PSP molecule in the solid state is (at least on average) planar, clearly intermolecular interactions play a role in determining the intramolecular torsion angles. These calculations address the issue of competition between the intramolecular forces in an isolated molecule and the intermolecular packing forces present within the crystal. Especially of interest is whether a double well potential results from these competitive effects in PSP, or if (unlike lower oligomers) one energy contribution dominates sufficiently to yield a single potential energy minimum.

Oligomer pairs

As a starting point, the interactions between pairs of oligomers were studied. The orientation angles (which will be identified as setting angles in a crystal) of the two molecules were varied, while both molecules were

Table 10 Bond distances (Å) and bond angles (deg) for *p*-septiphenyl

Atom 1	Atom 2	Distance	Atom 1	Atom 2	Distance	Atom 1	Atom 2	Distance
C1	C2	1.383(6)	C8	C9	1.386(6)	C15	H15	0.951(5)
C1	C3	1.379(5)	C8	H8	0.950(5)	C16	C17	1.392(6)
C1	C4	1.489(5)	C9	H9	0.951(4)	C16	C21	1.372(6)
C2	H2	0.950(4)	C10	C11	1.376(6)	C17	C18	1.407(6)
C3	H3	0.951(5)	C10	C15	1.377(6)	C17	H17	0.951(4)
C4	C5	1.382(5)	C11	C12	1.378(6)	C18	C19	1.369(7)
C4	C9	1.376(6)	C11	H11	0.951(6)	C18	H18	0.950(5)
C5	C6	1.383(6)	C12	C13	1.381(6)	C19	C20	1.375(7)
C5	H5	0.950(5)	C12	H12	0.950(5)	C19	H19	0.951(4)
C6	C7	1.389(7)	C13	C14	1.363(6)	C20	C21	1.406(6)
C6	H6	0.951(4)	C13	C16	1.499(5)	C20	H20	0.951(5)
C7	C8	1.376(6)	C14	C15	1.384(6)	C21	H21	0.951(4)
C7	C10	1.479(5)	C14	H14	0.950(5)	C2	C3'	1.384(4)
C3	C2'	1.384(4)						
Atom 1	Atom 2	Atom 3	Angle	Atom 1	Atom 2	Atom 3	Angle	
C2	C1	C3	116.3(3)	C12	C11	H11	118.9(4)	
C2	C1	C4	121.9(3)	C11	C12	C13	121.6(4)	
C3	C1	C4	121.8(3)	C11	C12	H12	119.6(5)	
C1	C2	C3'	121.9(3)	C13	C12	H12	118.9(5)	
C1	C2	H2	118.5(4)	C12	C13	C14	116.2(4)	
C1	C3	C2'	121.7(4)	C12	C13	C16	121.6(4)	
C1	C3	H3	119.2(4)	C14	C13	C16	122.2(4)	
C1	C4	C5	121.6(3)	C13	C14	H14	118.8(5)	
C1	C4	C9	121.9(3)	C15	C14	H14	118.8(4)	
C5	C4	C9	116.5(3)	C10	C15	C14	121.8(5)	
C4	C5	C6	122.1(5)	C10	C15	H15	118.5(4)	
C4	C5	H5	118.6(4)	C14	C15	H15	119.7(5)	
C6	C5	H5	119.4(5)	C13	C16	C17	121.0(4)	
C5	C6	C7	121.5(4)	C13	C16	C21	120.7(4)	
C5	C6	H6	119.4(5)	C17	C16	C21	118.3(3)	
C7	C6	H6	119.1(4)	C16	C17	C18	120.5(5)	
C6	C7	C8	116.2(3)	C16	C17	H17	119.9(4)	
C6	C7	C10	121.6(3)	C18	C17	H17	119.5(4)	
C8	C7	C10	122.2(4)	C17	C18	C19	119.7(5)	
C7	C8	C9	122.4(4)	C17	C18	H18	120.3(5)	
C7	C8	H8	118.2(4)	C19	C18	H18	120.0(5)	
C9	C8	H8	119.5(4)	C18	C19	C20	120.9(4)	
C4	C9	C8	121.6(4)	C18	C19	H19	119.3(5)	
C4	C9	H9	119.1(4)	C20	C19	H19	119.8(5)	
C8	C9	H9	119.3(4)	C19	C20	C21	118.8(4)	
C7	C10	C11	122.3(4)	C19	C21	H20	120.4(4)	
C7	C10	C15	122.0(3)	C21	C20	H20	120.8(5)	
C11	C10	C15	115.7(4)	C16	C21	C20	121.8(5)	
C10	C11	C12	122.5(4)	C16	C21	H21	119.2(4)	
C10	C11	H11	118.6(4)	C20	C21	H21	119.0(5)	

Numbers in parentheses are estimated standard deviations in the least significant digits

Table 11 Intersection angles and setting angles for *p*-polyphenyls

Compound	$\omega \pm 0.3^\circ$	$\theta \pm 0.3^\circ$	$\phi \pm 0.3^\circ$
Biphenyl	22.5	56	72.5
<i>p</i> -Terphenyl	19	57	73
<i>p</i> -Quaterphenyl	11.5	56.5	73
<i>p</i> -Quinquephenyl	9.5	56.5	73
<i>p</i> -Sexiphenyl	26	55	71
<i>p</i> -Septiphenyl	6.5	57	72.5

constrained to the same phenyl–phenyl torsion angles. Shown in *Figure 14* is a projected view (parallel to the molecular axis) of the PSP unit cell. For convenience, the molecular (projection) axis can be identified as *a'* ($=b \times c$). Intermolecular energies were calculated for the oligomers marked 1 and 2. The orientation angles Θ_1 and Θ_2 were varied independently in 20° increments over the unique range of 0 – 180° . The calculations were repeated for oligomers having torsion angles from 0 to

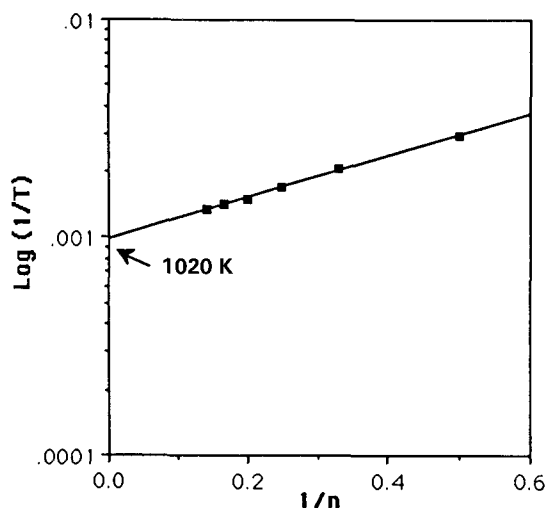
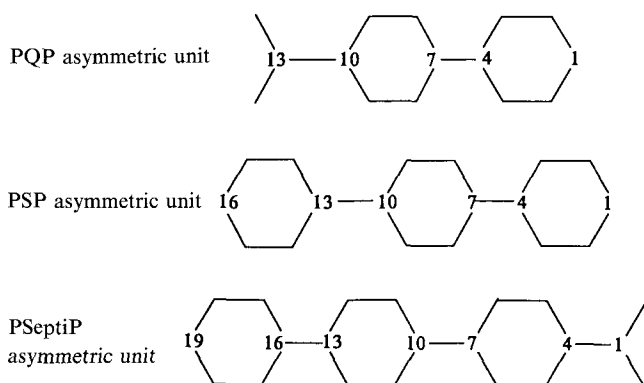
90° (in 10° intervals) and at intermolecular distances from 3.25 to 7.0 Å (in increments of 0.25 Å).

The contour map in *Figure 15a* shows the intermolecular energy as a function of the orientation angles. At orientation angles $\Theta_1=0$ and $\Theta_2=0$, the planes of the oligomers are parallel to each other and to the *a'c* plane of the unit cell. The energy values correspond to the intermolecular energy between oligomers having the torsion angles and separation distances which gave the overall lowest energy for that particular combination of orientation angles. *Figure 15b* shows the torsion angles which gave the lowest energy for each combination of orientation angles, and *Figure 15c* shows the corresponding minimum energy separation distances. The separation distances correlate nicely with the packing energy. Comparing *Figures 15b* and *c*, it can be seen that for a separation distance of between 4.5 and 5.0 Å, there are reasonably low-energy orientations, even for molecules having torsion angles of 90° .

The torsion angle contour plot shown in *Figure 15b* is presented three-dimensionally in *Figure 16*. Besides the

Table 12 Angles ($^{\circ}$) between molecular axis carbon atoms

	Atoms	Angles
PQP	C1-C4-C7	179.5
	C4-C7-C10	178.5
	C7-C10-C13	179.5
	C10-C13-C13'	178.7
PSP	C1'-C1-C4	176.4
	C1-C4-C7	178.2
	C4-C7-C10	177.6
	C7-C10-C13	178.3
PSeptiP	C10-C13-C16	178.0
	C1'-C1-C4	179.6
	C1-C4-C7	179.8
	C4-C7-C10	178.2
	C7-C10-C13	178.0
	C10-C13-C16	179.2
	C13-C16-C19	178.1

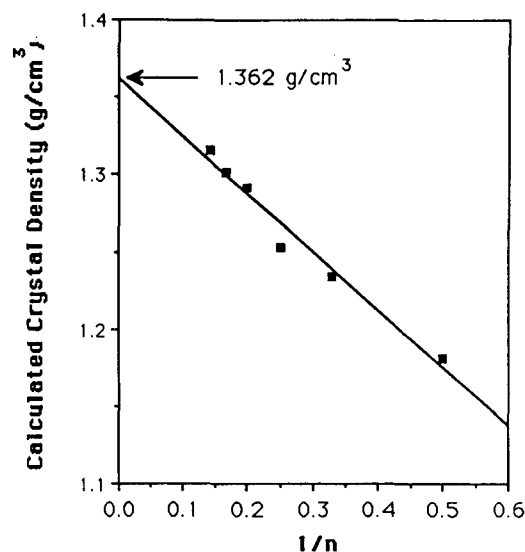
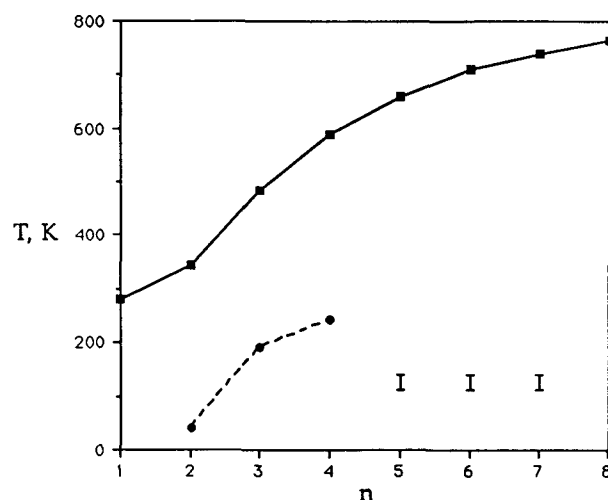
**Figure 8** Reciprocal oligomer length versus the logarithm of reciprocal temperature, showing the extrapolation to obtain an estimate of the melting temperature of PPP

plateau region at torsion angles of 0–10°, there is also a plateau at torsion angles around 40–50° (for $\Theta_1 > 100^\circ$ and Θ_2 between 20 and 100°). Interestingly, efficient packing modes are also available to molecules with 90° torsions as shown by the presence of a third plateau corresponding to 80–90° torsions.

From these data, low-energy relationships and the corresponding conformational geometries can be determined for a pair of oligomers. The most energetically favourable relationships, itemized in Table 13, occur largely when the phenyl-phenyl torsion angles are 0 or

10°. Molecules related to each other as are 1 and 2 in Figure 14 will have orientations located in the lower left quadrant of the maps shown in Figure 15, i.e. with Θ_1 and Θ_2 between 0 and 90°. In this region, torsion angles of 0 or 10° account for the minima at 70% of the sets of orientation angles. The other dominant torsion angle is 50°, accounting for the minima at 22% of the sets of orientation angles. However, these latter orientations have intermolecular energies at least 8 kcal mol⁻¹ higher than the lowest energy arrangements. Bearing in mind that the lowest energy torsion angle for an isolated molecule is approximately 30°, these results indicate that the general effect of intermolecular forces is toward restoring planarity in order to lower the packing energy.

The results also indicate that the most favourable angular relationships occur when the oligomers have orientation angles between 0 and 20° with respect to the *a**c* plane of the unit cell shown in Figure 14. The crystal structure, however, juxtaposes molecules with orientation

**Figure 9** Reciprocal oligomer length versus calculated crystal density, showing the extrapolation to obtain an estimate of the crystalline density of PPP**Figure 10** Melting temperatures (—■—) and structural transition temperatures (---●---) versus oligomer length. Error bars are shown for $n=5, 6$ and 7

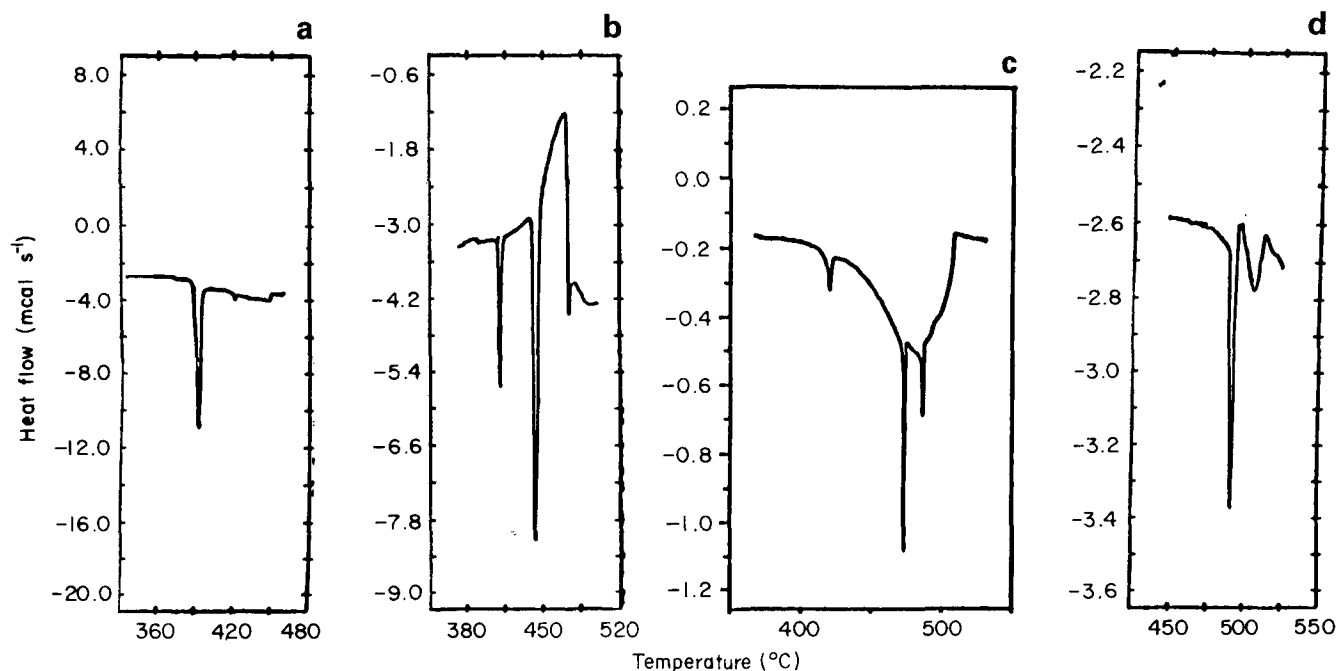


Figure 11 D.s.c. measurements for (a) PQP, (b) PSP, (c) PSeptiP and (d) POP. The scan rate was $10^{\circ}\text{C min}^{-1}$

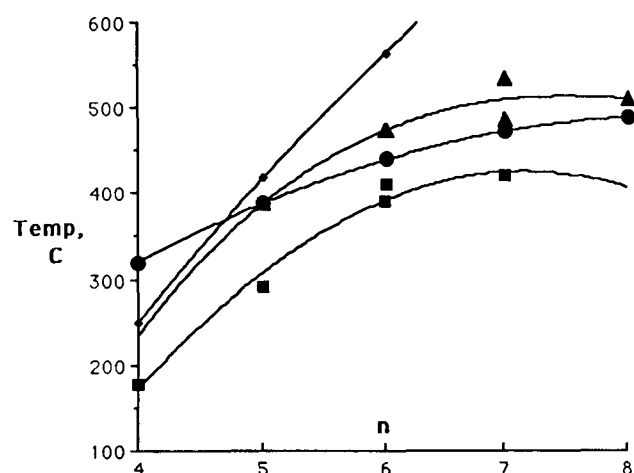


Figure 12 Liquid crystal phase transition temperatures versus oligomer length: ■, crystal-crystal; ●, crystal-smectic; ▲, smectic-nematic; ◆, nematic-isotropic

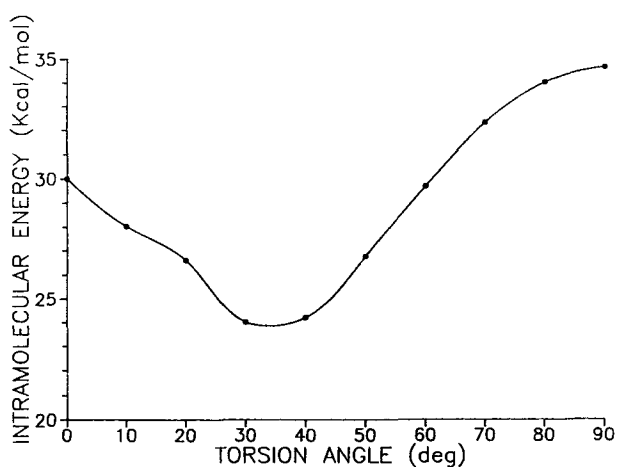


Figure 13 Intramolecular energy versus torsion angle for PSP

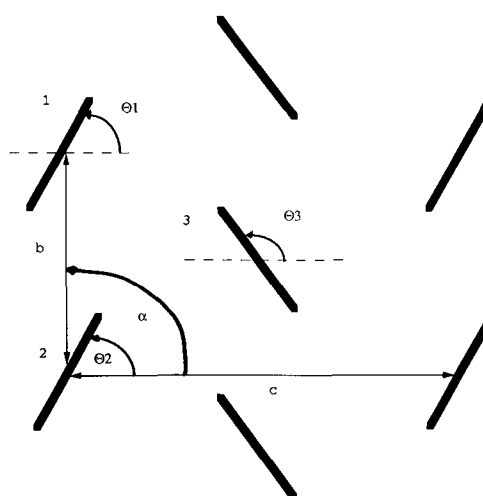
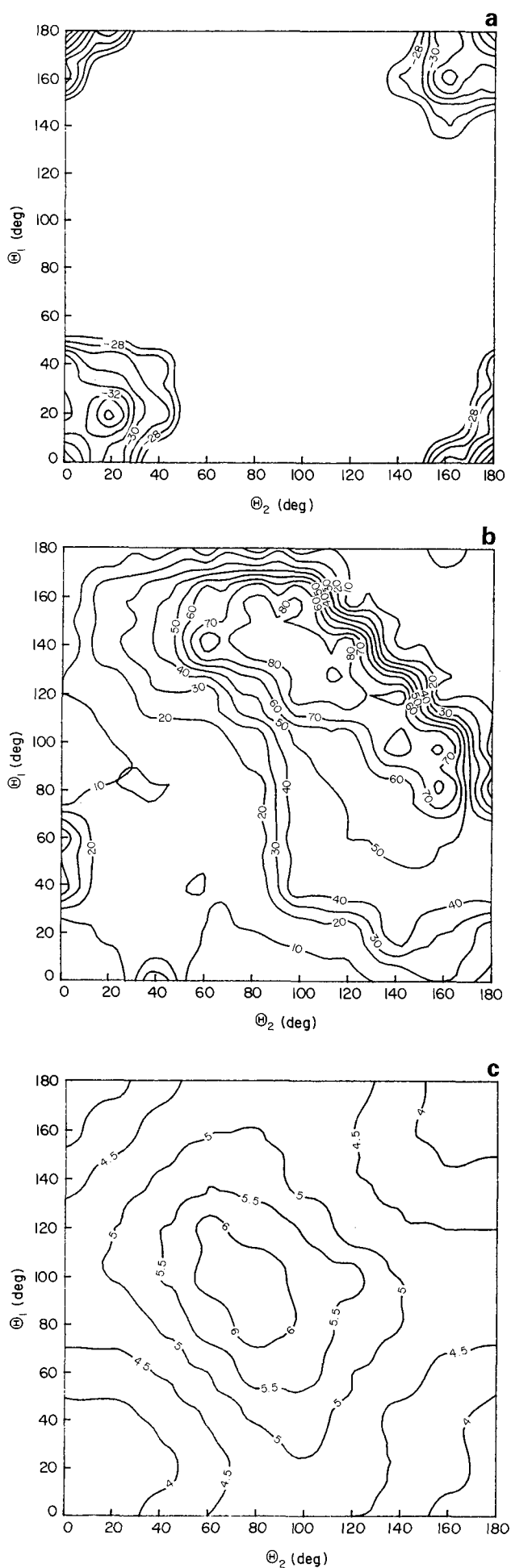


Figure 14 Schematic view of PSP unit cell projected along the molecular axis

angles of $\Theta_1 = \Theta_2 = 60^{\circ}$, at which the intermolecular energy, $-18 \text{ kcal mol}^{-1}$, is only half that of the minimum value, and torsion angles of 10° are preferred. In the context of the pairwise contour maps, the interactions between oligomers 1 and 3 or between oligomers 2 and 3 (in Figure 14) occur at about $\Theta_2 = 130^{\circ}$ and $\Theta_3 = 10^{\circ}$, for instance. The corresponding optimum torsion angles are 0 to 10° and the energy is about $-23 \text{ kcal mol}^{-1}$. Clearly, the structure must compromise individual pairwise interactions in favour of optimizing the interactions between all the neighbours of a given oligomer. Consideration of pairwise interaction alone, though instructive vis-a-vis intra- versus intermolecular interactions, does not lead unambiguously to structures such as are found in the crystal.

The effects of translations parallel to the molecular axis were also investigated. Pairs of PSP oligomers constrained to the same phenyl-phenyl torsion angle (ranging from 0 to 90° in 10° intervals) were translated



with respect to one another in fractional increments of the chain repeat unit ($=4.32 \text{ \AA}$). Intermolecular distances were also varied and optimized at each translation. Results are shown in *Figure 17*. By far the most favourable relationships were achieved when each oligomer was constrained to have phenyl-phenyl torsion angles of 0° (planar) or 10° . In each case, the optimum separation distance was 3.5 \AA . Translations along the molecular axis greater than approximately 1.5 \AA significantly increased the intermolecular energy. Low-energy packing relationships correspond to translations between 1.1 and 1.3 \AA for oligomers constrained to torsions of 0 or 10° . X-ray data indicate a crystallographic translation of approximately 1.5 \AA between oligomers in the lattice.

The increase in intermolecular energy with translation (shown in *Figure 17*) includes a significant end-effect due to the computational model. Any possible lowering of the energy by translation is overcome by the loss of intermolecular interactions at the ends of the oligomers. To gain an estimate of the magnitude of this end-effect and determine the optimum translation in the crystalline environment, a second model was used. In this model, the intermolecular energy of a central ring of one planar PSP oligomer was calculated as it was translated (parallel to the molecular axis) past a second planar oligomer. The energy of the central ring is not significantly affected by intermolecular attractions lost from the end of the molecule during translation. The energy calculated in this fashion is nearly constant for translations between 1.7 and 2.4 \AA , and over the entire range of translations varies by only $0.25 \text{ kcal mol}^{-1}$. These results suggest that the packing of the chain ends in the crystal can play a significant role in determining the actual translation value observed in the crystal.

Packing of seven PSP oligomers

To study the influence of intermolecular interactions on the torsion angles adopted by PSP oligomers in the solid state, calculations on an array of PSP oligomers were carried out. The intermolecular energy of the central oligomer in *Figure 14* with its surrounding molecules was calculated. All PSP oligomers were constrained to the same phenyl-phenyl torsion angle. The unit cell dimensions b , c and a , as well as the setting angles Θ_1 and Θ_2 , were varied simultaneously and optimized for each particular conformation of the seven oligomers. Increments of 0.1 \AA in the cell dimensions, 1° for the cell angle, and 5° for the setting angle were used. Translations between molecules were not considered initially in the optimizations. Intermolecular energies are presented in *Figure 18*. The minimum intermolecular energy for the oligomers in the lattice corresponds to a packing mode in which the molecules have all their member phenyl rings coplanar.

In *Figure 19*, the total energy (inter- + intramolecular) of the central oligomer in *Figure 14* is plotted versus phenyl-phenyl torsion angle. The most favourable

Figure 15 (a) Energy contour map for a pair of PSP molecules having orientation angles Θ_1 and Θ_2 . For each pair of angles, the energy value (kcal mol^{-1}) corresponds to that of the lowest energy separation distance and phenyl-phenyl torsion angle. (b) Contour map showing the optimum phenyl-phenyl torsion angle (deg) for a pair of PSP molecules having orientation angles Θ_1 and Θ_2 . (c) Contour map showing the minimum energy separation distance (\AA) for a pair of PSP molecules having orientation angles Θ_1 and Θ_2 .

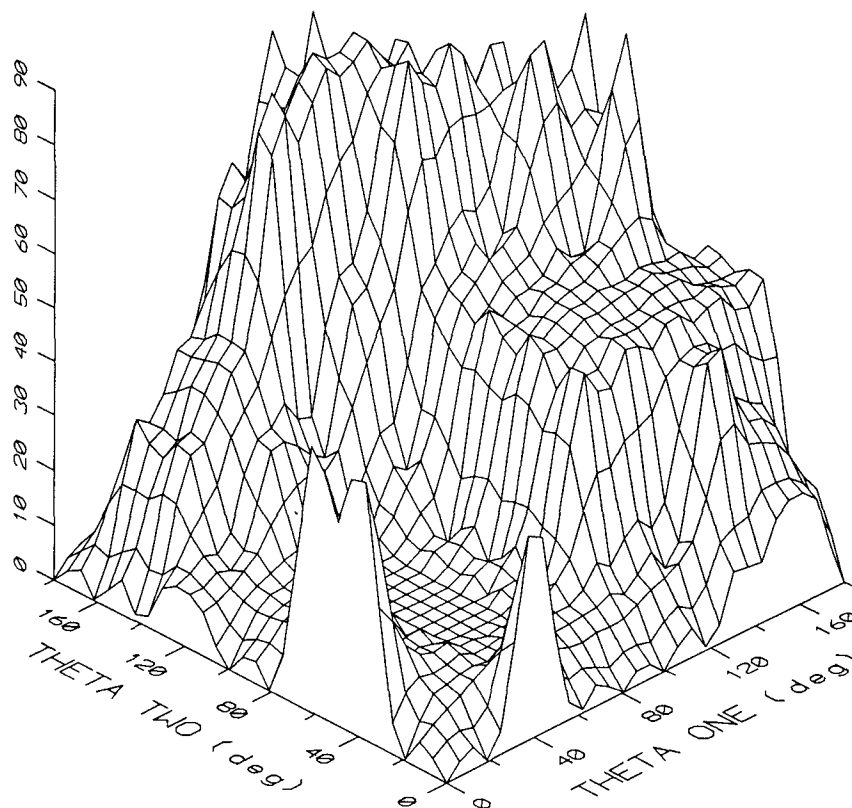


Figure 16 Three dimensional plot showing the optimum phenyl-phenyl torsion angle for a pair of PSP molecules having orientation angles Θ_1 and Θ_2

Table 13 Low energy orientations for oligomers 1 and 2

Oligomer torsion angle (deg)	Θ_1 (deg)	Θ_2 (deg)	Intermolecular energy (kcal mol ⁻¹)
0	0	0	-35.18
10	20	20	-34.72
50	0	40	-31.85
0	0	20	-30.70
10	40	20	-29.99
10	40	40	-28.93

relationship in the array occurs when the oligomers are all planar. Comparing these results to those shown for an isolated PSP oligomer (Figure 13), it is clear that intermolecular forces present within the lattice are sufficient to overcome intramolecular energies and that the competition between inter- and intramolecular energies is dominated by the intermolecular contribution to the energy. The energy curve (Figure 19) shows a single minimum at 0°, rather than showing one of a pair of symmetrically related minima at a phenyl-phenyl torsion angle offset from 0° (as would be the case were there a double minimum). While likely to be sensitive to the scaling between non-bonded energy contributions (which constitute the intermolecular energy) and the bond deformation energies (which account primarily for the intramolecular energy), this result suggests that the observed planar structure in PSP might not be a consequence of 'averaging' over two symmetrically disposed conformational states. However, since the energies calculated by molecular mechanics correspond to internal energies, other contributions to the free energy may alter this result. Molecular dynamics simulations, which are currently underway, should provide further

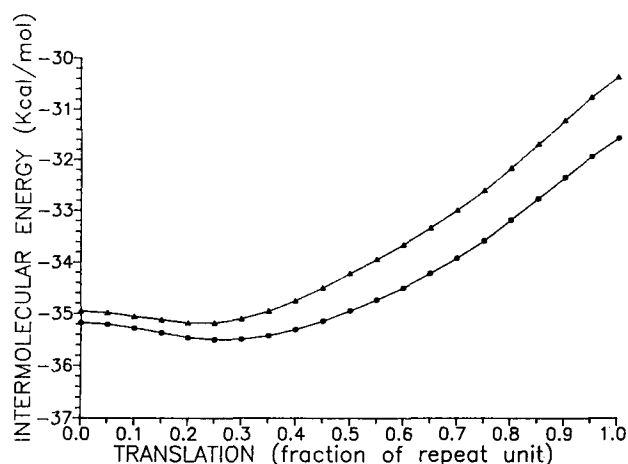


Figure 17 Intermolecular energy for a pair of PSP molecules versus translation parallel to their axes: ●, planar molecules; ▲, molecules having torsion angles of 10°

insight into this aspect of the structure of PSP and related materials.

Conformations having small phenyl-phenyl torsion angles are preferred within the confines of the crystal. This balance should not be altered significantly by changes in molecular length. The addition of phenyl groups would incrementally change both the intramolecular torsion energy and intermolecular packing energy. Experimentally observed changes in structure with increasing oligomer length may reflect the diminishing influence of packing the chain ends vis-a-vis the central portions of the molecules.

The calculated unit cell dimensions and setting angles for arrays of oligomers with torsion angles of 0, 10 and 20° are shown in Table 14. The results are

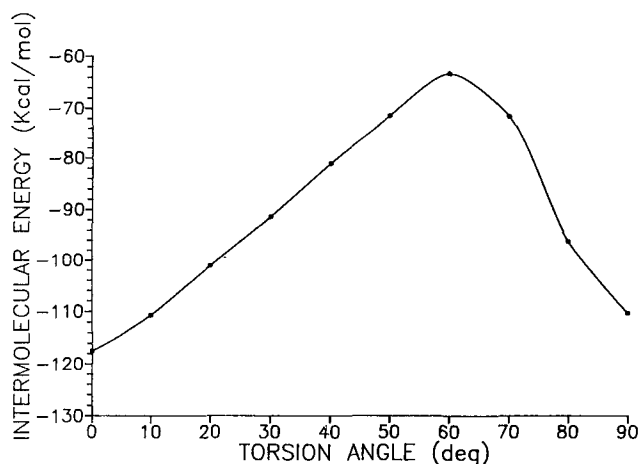


Figure 18 Intermolecular energy for a seven-molecule array of PSP molecules versus phenyl-phenyl torsion angle of the PSP molecules

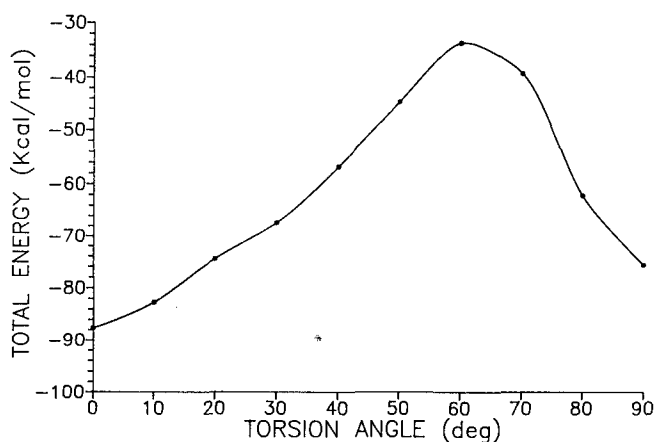


Figure 19 Total energy (intramolecular + intermolecular) for a seven-molecule array of PSP molecules versus torsion angle

Table 14 Calculated and experimental unit cell data

Oligomer torsion angle (deg)	<i>b</i> (Å)	<i>c</i> (Å)	α (deg)	Θ_1 (deg)	Θ_3 (deg)
0	5.2	7.8	90	60	125
10	5.3	7.8	90	65	130
20	5.6	7.8	90	50	120
Experiment	5.568 ^a	7.73 ^a	90	60	125

^a Measured normal to the molecular axes

generally in good agreement with experimental values. Underestimation of the *b* cell dimension calculated for the planar oligomers and the calculated increase in *b* for other torsion angles suggests that librations could account for the larger observed value.

Translations in the lattice

As previously noted, a crystallographic translation of approximately one-half of a phenyl ring (1.5 Å) is observed in the crystal structure of PSP. Translations in a crystalline environment (such that necessary crystalline relationships were preserved) were investigated for molecules having phenyl-phenyl torsion angles of 0° (planar) and 10°. Results are shown in Figure 20. In each case, a crystallographic translation along the molecular

axis of up to 1.3 Å lowers the intermolecular energy of the central oligomer in Figure 14. Further translation, however, increases the intermolecular energy. This again indicates that a translation within the lattice will lower the energy, until end-effects of the model begin to overcome any stability gained by introducing further translation.

To minimize end-effects, the intermolecular energy of a central phenyl ring (in the central oligomer of Figure 14), was calculated as a function of crystallographic translation along the molecular axis. The results are given in Figure 21. The period of the energy curve corresponds to a translation along the molecular axis of one phenyl unit. (The slight asymmetry of the curve with respect to a translation of half of a repeat unit is due to the use of X-ray coordinates to build the molecules. As noted earlier, these coordinates leave the phenyl groups of the PSP molecule not quite identical and the molecule with a slight bend at its centre.) The intermolecular energy minimum calculated with this model occurs at a translation distance of approximately 1.5 Å, in excellent agreement with X-ray results. This slightly larger translation distance, as compared to the preceding calculation, shows the importance of lost intermolecular attractions at the ends of the oligomers. In a crystal, the

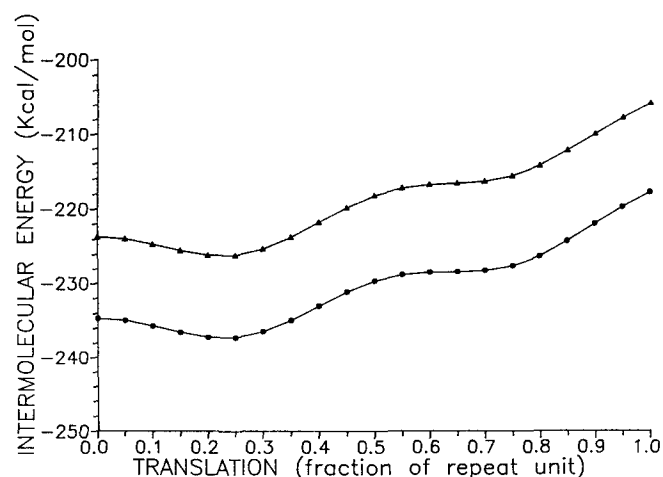


Figure 20 Intermolecular energy for a seven-molecule array of PSP molecules versus crystallographic translation parallel to the molecular axis: ●, planar molecules; ▲, molecule having torsion angles of 10°

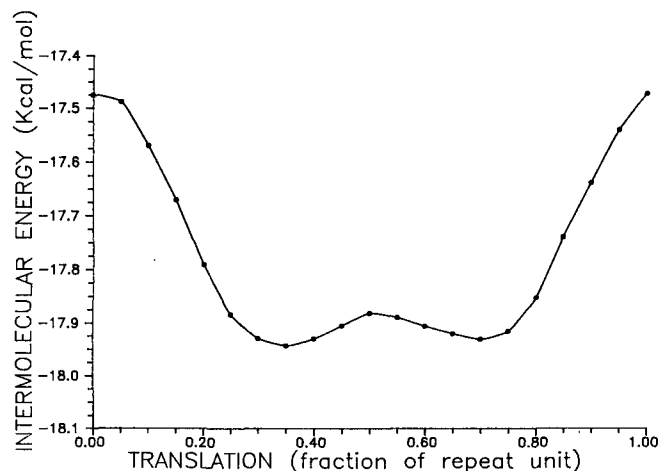


Figure 21 Intermolecular energy for a central phenyl ring versus crystallographic translation parallel to the molecular axis

periodicity of the lattice offsets these intermolecular interactions lost in the computational model.

CONCLUSIONS

The structures of the 5-, 6- and 7-ring oligomers of PPP follow the same pattern as shorter oligomers previously studied. The unit cell parameters are very similar, with the exception of the *a* crystallographic axis which increases with oligomer length to accommodate the longer chain. All the oligomers belong to similar space groups, and have similar bond lengths and bond angles. Linear, planar molecules are observed in all three structures, but the herringbone packing of the molecules in the structures is different. The even-numbered oligomer is skewed in the unit cell much more than the odd-numbered oligomers. The setting angle for the oligomers matches that of PPP.

Low temperature transitions for PQP, PSP and PSeptiP occur between 110 and 140 K and are time dependent. Detailed molecular structures could not be resolved, nor could transition temperatures be pinpointed. Liquid crystal transitions were also observed near the melting temperatures, but sample decomposition above 500°C precluded detailed study.

Results from molecular mechanics calculations clearly show the effects of intermolecular packing forces on the torsion angles of the molecules. When isolated, PSP oligomers adopt non-planar conformations. In a crystalline environment, planar or nearly planar conformations are favoured. Calculated unit cell dimensions, setting angles, oligomer conformations and crystallographic translations are in good agreement with X-ray results. The results suggest that the total internal energy for PSP has a single minimum corresponding to packing of planar oligomers. No evidence of a double-well potential, such as postulated for *p*-terphenyl, is observed. The results also indicate that the observed translations of the molecules in the crystal are significantly influenced by end-group packing within the layered oligomer structures.

REFERENCES

- Noren, G. K. and Stille, J. K. *J. Polym. Sci. Macromol. Rev.* 1971, **5**, 385
- Speight, J. G., Kovacic, P. and Koch, F. W. *J. Macromol. Sci. Rev. Macromol. Chem.* 1971, **5**, 295
- Kovacic, P. and Jones, M. B. *Chem. Rev.* 1987, **87**, 357
- Unroe, M. R. and Reinhardt, B. A. *Synthesis* 1987, **11**, 981
- Martinek, T. W., Haines, R. M., Weichman, R. L. and Trainor, W. J. US Patent 3 476 687, 1969; *Chem. Abstr.* 1969, **72**, 14472d
- McMahon, M. A. Jr, Chafez, H. and Coppoc, W. J. US Patent 3 384 588, 1968; *Chem. Abstr.* 1968, **69**, 20938q
- McCarthy, P. R. and Tempalski, C. S. US Patent 3 291 733, 1966; *Chem. Abstr.* 1966, **66**, 57627b
- Agnew, R. J. and Dille, K. L. US Patent 3 278 429, 1966; *Chem. Abstr.* 1966, **66**, 12765d
- Accountis, O. E. US Patent 3 443 899, 1969; *Chem. Abstr.* 1969, **71**, 22829v
- Sato, M., Yamazaki, H. and Yamaguchi, S. Japan Patent 63/102 982, 1988; *Chem. Abstr.* 1988, **109**, 160647p
- Gale, D. M. *J. Polym. Sci., Polym. Lett. Edn* 1977, **15**, 439
- Gale, D. M. *J. Appl. Polym. Sci.* 1978, **22**, 1955
- Ostrum, G. K., Lawson, D. D. and Ingham, J. D. *Polym. Prepr.*, 1966, **7**, 895
- Wierschke, S. G. in 'The Materials Science and Engineering of Rigid-Rod Polymers', (Eds W. W. Adams, R. K. Eby and D. E. McLemore) Materials Research Society Proceedings no. 134, Boston, 1988, p. 313; AFWAL-TR-88-4201, 1988
- Wierschke, S. G., Shoemaker, J. R., Haaland, P. D., Pachter, R. and Adams, W. W. *Polymer* submitted
- Ivory, D. M., Miller, G. G., Sowa, J. M., Shacklette, L. W., Chance, R. R. and Baughman, R. H. *J. Chem. Phys.* 1979, **71**, 1506
- Pradere, P. and Boudet, A. *J. Mater. Sci. Lett.* 1988, **7**, 10
- Baughman, R. H., Shacklette, L. W., Murthy, N. S., Miller, G. G. and Elsebaumer, R. L. *Mol. Cryst. Liq. Cryst.* 1985, **118**, 253
- Dory, M., Bodart, V. P., Delhalle, J., Andre, J. M. and Bredas, J. L. in 'Nonlinear Optical Properties of Polymers' (Eds A. J. Heeger, J. Orenstein and D. R. Ulrich) Materials Research Society Proceedings no. 109, Pittsburgh, 1988, p. 239
- Bredas, J. L., Chance, R. R. and Baughman, R. H. *J. Chem. Phys.* 1982, **76**, 3673
- Bredas, J. L., Dory, M., Themans, B., Delhalle, J. and Andre, J. M. *Synth. Met.* 1989, **28**, D553
- Leising, G., Leitner, O., Aldrian, F. and Kahlert, H. *Synth. Met.* 1987, **17**, 635
- Bredas, J. L. *J. Chem. Phys.* 1985, **82**, 3208
- Bredas, J. L., Themans, B., Tripiat, J. G., Andre, J. M. and Chance, R. R. *Phys. Rev. B: Condens. Matter* 1984, **29**, 6761
- Yi, X., Xiaoming, L. and Duanming, Z. *J. Mol. Sci.* 1987, **5**, 229
- Pelous, Y., Froyer, G., Herold, C. and Lefrant, S. *Synth. Met.* 1989, **29**, E17
- Kispert, L. D., Joseph, J., Miller, J. J. and Baughman, R. H. *J. Chem. Phys.* 1984, **81**, 2119
- Irvine, P. A., Wu, D. C. and Flory, P. J. *J. Chem. Soc., Faraday Trans. I* 1984, **80**, 1795
- Flory, P. J. and Ronca, G. *Mol. Cryst. Liq. Cryst.* 1979, **54**, 311
- Smith, G. W. *Mol. Cryst. Liq. Cryst. Lett.* 1979, **49**, 207
- Desiraju, G. R. and Gavezzotti, A. *Acta Crystallogr.* 1989, **B45**, 473
- Baudour, J. L., Delugeard, Y. and Rivet, P. *Acta Crystallogr.* 1978, **B34**, 625
- Baudour, J. L. *Acta Crystallogr.* 1991, **B47**, 935
- Baker, K. N., Knachel, H. C., Fratini, A. V. and Adams, W. W. in 'The Materials Science and Engineering of Rigid-Rod Polymers' (Eds W. W. Adams, R. K. Eby and D. E. McLemore) Materials Research Society Proceedings no. 134, Boston, 1988, p. 497
- Cailleau, H., Baudour, J. L., Meinnel, J., Dworkin, A., Moussa, F. and Zeyen, C. M. E. *Faraday Discuss. Chem. Soc.* 1980, **69**, 7
- Tsuzuki, S. and Tanabe, K. *J. Phys. Chem.* 1991, **95**, 139
- Frenz, B. A. and Associates, Inc., College Station, TX, and Enraf-Nonius, Delft, The Netherlands, Structure Determination Package, 1985
- Main, P. (Ed.) 'MULTAN 11/82, A System of Computer Programs for the Automatic Solution of Crystal Structures from X-ray Diffraction Data', Department of Physics, University of York, 1982
- Sheldrick, G. M. in 'Crystallographic Computing 3' (Eds G. M. Sheldrick, C. Fruger and R. Goddard), Oxford University Press, Oxford, 1985, pp. 175-189
- SYBYL, Version 5.4, Tripos Associates, St. Louis, MO, 1991
- Clark, M., Cramer III, R. D. and Van Opdenbosch, M. *J. Comput. Chem.* 1989, **10**, 982
- Farmer, B. L., Chapman, B. R., Dudis, D. S. and Adams, W. W. *Polymer* 1993, **34**, 1588
- Farmer, B. L. MS Thesis, Case Institute of Technology, 1972
- Sorensen, R. A., Liau, W. B., Kesner, L. and Boyd, R. H. *Macromolecules* 1988, **21**, 200
- SURFER, Version 4, Golden Software Corp., Golden, CO, 1989
- Charbonneau, G.-P. and Delugeard, Y. *Acta Crystallogr.* 1977, **B33**, 1586
- Baudour, J. L., Delugeard, Y. and Sanquer, M. *Acta Crystallogr.* 1974, **B30**, 691
- Delugeard, Y., Desuche, J. and Baudour, J. L. *Acta Crystallogr.* 1976, **B32**, 702
- Kawaguchi, A. and Petermann, J. *Mol. Cryst. Liq. Cryst.* 1986, **133**, 189
- Seki, K., Kailsson, U. O., Engelhardt, R., Koch, E.-E. and Schmidt, W. *Chem. Phys.* 1984, **91**, 459
- Kovacic, P. and Kyriakis, A. *J. Am. Chem. Soc.* 1963, **85**, 454
- Flory, P. J. 'Principles of Polymer Chemistry', Cornell University Press, Ithaca, 1953, p. 570
- Starkweather, H. W. *Macromolecules* 1986, **19**, 1131
- Gardner, K. personal communication, 1989
- Cailleau, H., Baudour, J. L. and Zeyen, C. M. E. *Acta Crystallogr.* 1979, **B35**, 426
- Cailleau, H. and Dworkin, A. *Mol. Cryst. Liq. Cryst.* 1979, **50**, 21

- 57 Bree, A. and Edelson, M. *Chem. Phys. Lett.* 1977, **46** (3), 500
58 Lewis, I. C. and Barr, J. B. *Mol. Cryst. Liq. Cryst. Lett.* 1981, **72**, 65
59 Wunderlich, B., Moller, M., Grebowicz, J. and Baur, H. *Adv. Polym. Sci.* 1988, **87**, 67
60 Windle, A. *MRS Bull.* 1987, **12**, 18
61 Toudic, B., Gullieu, J., Rivet, P. and Delugeard, Y. *Chem. Phys.* 1985, **99**, 275
62 Dumais, J. J., Jelinski, L. W., Galvin, M. E., Dybowski, C., Brown, C. E. and Kovacic, P. *Macromolecules* 1989, **22**, 612
63 Kern, W., Ebersbach, H. W. and Ziegler, I. *Makromol. Chem.* 1959, **31**, 154
64 Unroe, M. R. and Reinhardt, B. A. *Synthesis* 1987, **11**, 981
65 Kambe, H., Mita, R. and Yokota, R. *Thermal Anal.* 1971, **3**, 387
66 Bolton, B. A. and Prasad, P. N. *Chem. Phys.* 1978, **35**, 331